JOURNAL OF CATALYSIS 96, 314–325 (1985)

EXAFS Study of Cu–ZnO/Al_2O_3 Catalysts for the Low-Temperature CO Shift Reaction

G. VLAIC,* J. C. J. BART,*,[1] W. CAVIGIOLO,* B. PIANZOLA,* S. MOBILIO†

*Istituto G. Donegani S.p.A., Via G. Fauster 4, 28100 Novara, and †Laboratori Nazionali di Frascati, INFN, Gruppo PULS, Frascati, Italy

Received October 14, 1983; revised September 7, 1984

EXAFS measurements by means of synchrotron radiation of Cu–ZnO/Al_2O_3 CO shift catalysts and various reference compounds (Cu, CuO, Cu_2O, ZnO, and spinels) show the presence of CuO and ZnO in fresh catalysts and of highly dispersed Cu and ZnO after activation and reduction. The presence of Cu_2O and spinels is excluded within the detection limits. The results are in agreement with previously reported XANES studies of the same catalyst samples. © 1985 Academic Press, Inc.

INTRODUCTION

Interaction of CO with water vapor (low-temperature CO shift reaction, LTS) on copper-zinc oxide/alumina catalysts at low-temperature (180–250°C) is widely used in hydrogen plants for ammonia synthesis and hydrogenation processes (*1*). The role of the various components of such catalysts, or of similar systems in use for methanol synthesis, has recently been extensively studied by a variety of experimental techniques (*2–6*). The question of the composition and structure of the main active phase is obviously of interest because the low-temperature catalyst is rather unstable in relation to the effect of the reaction medium, temperature and sensitivity to catalytic poisons.

The high activity of the catalysts is due to the action of a copper (20–50 wt% as oxide)–zinc couple. In the initial activated state (fresh catalysts), copper is mainly in a divalent state. However, the catalyst operates in a reduced state, which is reached by treatment with H_2 or CO at about 200°C. Under these conditions CuO is reduced to copper rather than Cu_2O, as occurs under vacuum conditioning treatments (*7*), whereas zinc oxide remains apparently unvaried at this temperature. In a reducing gas above 250°C brass can be formed in the Cu–ZnO catalyst (*8*). With intimate admixture of the catalyst components (as for coprecipitated catalysts) dissolution of copper in the zinc oxide phase has been claimed (*3, 4*).

The present investigation aims at studying the composition of some fresh and reduced catalysts. As the usual degree of dispersion of the active phase(s) on the amorphous support (typically about 100 Å for the coprecipitated catalysts after activation by reduction) (*1, 9–14*) is an obstacle to many of the traditional methods of structural investigation, we have chosen the extended X-ray absorption fine structure technique (EXAFS) for the study of the catalyst composition. The advantage is that EXAFS data analysis is independent of structural order.

EXPERIMENTAL

Materials. Cu_2O, CuO, and ZnO were R. P. C. Erba products; Cu and Zn were available as sheets (20 × 10 × 0.004 mm) from Goodfellow Metals, Ltd., $ZnAl_2O_4$ was prepared as described in Ref. (*14*).

Cu–ZnO/Al_2O_3 catalysts were either commercially available products or samples prepared on alumina by hot precipita-

[1] Present address: Institut de Recherches sur la Catalyse (CNRS), 2 Avenue A. Einstein, 69626 Villeurbanne, France.

0021-9517/85 $3.00

tion of nitrates in aqueous solution with sodium carbonate. Reduction of the catalysts was carried out with a 0.5–3% H_2 in N_2 gas mixture (p = 1 atm; space velocity = 50,000 h^{-1}) in a microflow apparatus for about 14 h at temperatures from 25 to 230°C. Composition and physicochemical characteristics of the three ternary catalysts are given in Table 1 (cf. Ref. (*14*)). Fresh and activated (reduced) catalysts are distinguished by a suffix F or R, respectively. Powder samples for EXAFS experiments were mixed with a diluent (BN) and pressed as tablets with thickness such as to optimize the contrast at the high-energy side of the absorption edge. Activated samples were kept in inert atmosphere (purified He) throughout the experiments.

Data collection. EXAFS spectra of both Cu and Zn were recorded at the Synchrotron Radiation Facility (PULS) at the Frascati National Laboratories (INFN), Italy, using the X-ray beam line. The experimental apparatus has been described elsewhere (*15*). The X-rays emitted by the ADONE storage ring at 1.5 GeV with a typical current of 50 mA were monochromatized by a channel-cut Si(220) single crystal and monitored (as I_0) in a first transmission ionization chamber filled with a He/N_2 mixture. After passing through the sample, the beam intensity I was measured by a second, total absorbing ionization chamber filled with a N_2/Ar mixture. The apparatus was operated under control of a PDP 11/03 minicomputer which drives the shafts of the monochromator and records the digitized currents I_0 and I.

All EXAFS spectra were taken at room temperature, in air for the standards and the fresh catalysts and in inert atmosphere for the activated catalysts. Measurements were made in about 2-eV intervals (with fixed angular step) over a scan range of about 1150 eV, extending up to 750 eV above the K thresholds of Cu and Zn, with an integration time of 1 s. Calibration of the energy scale E_0 was performed by attribution of literature values (*16*) to the maxima in the first-derivative edge spectra of metallic Cu and Zn (E_K^0 (Cu) = 8980.3 eV, E_K^0 (Zn = 9660.7 eV).

Data handling. The data are described as a measurement of the X-ray linear absorption coefficient μ in terms of the incident beam I_0, the transmitted intensity I, and the sample thickness x, as

$$\mu x = \ln \frac{I_0}{I}. \tag{1}$$

The EXAFS modulation of the absorption above the edge is given by

$$\chi(k) = \frac{\mu(k) - \mu_B(k) - \mu_0(k)}{\mu_0(k)}, \tag{2}$$

where μ_0 is the smooth, atom-like contribution and μ_B the background (originating from preedge absorption processes), k is the photoelectron wave vector:

TABLE 1

Cu–ZnO/Al_2O_3 Catalysts Investigated

Sample designation	Composition[a] (wt%)	Phase analysis	Crystallite size (Å)	
			CuO(111)	ZnO(110)
Cat. 1	24:47:15	CuO, ZnO	66	94
Cat. 2	29:45:12	CuO, ZnO, other[b]	—	—
Cat. 3	27:52:12	CuO, ZnO, other[b]	87	115

[a] CuO : ZnO : Al_2O_3; remainder consists of volatiles (H_2O, CO_2, etc.).
[b] Small amounts.

$$k = \left[\frac{2m}{\hbar^2}(E - E_0)\right]^{1/2}. \quad (3)$$

Here E is the incident photon energy, E_0 the photoelectron binding energy, m the electron rest mass, and $\hbar$ relates to Planck's constant. (We notice that the reference energy E_0 was fixed, with an arbitrary but uniform choice, at the inflection points of the K-edges of Cu and Zn; the values are listed in Table 2 of Ref. (*14*)). The simple backscattering theory gives the relationship between $\chi(k)$ and the structural parameters (*17*):

$$k\chi(k) = \sum_i \frac{N_i}{R_i^2} \exp(-2\sigma_i^2 k^2) \cdot F_i(k) \sin[2kR_i + \psi_i(k)], \quad (4)$$

where R_i is the average distance which separates the absorbing atom from the N_i neighboring atoms defining the ith shell, with a rms deviation σ_i; $F_i(k)$ and $\psi_i(k)$ are the amplitude backscattering factor and phase shift, respectively, characteristic of the selected atom pair. Data processing was carried out on a UNIVAC 1100/20 computer according to our standard procedure (*18, 19*), briefly summarized as follows:

(i) $\mu_B(k)$ is extrapolated from the preedge region where a Victoreen fit (*20*) has been used and subtracted from the experimental data. $\mu_0(k)$ was obtained by means of a Fourier filtering technique, not zeroing the high frequencies of noise (*18*).

(ii) the k-weighted EXAFS spectra were then Fourier-transformed (FT) from k-space to R-space using a Gaussian window. For all Cu-containing samples a back-Fourier transform (FT^{-1}) was then applied to the first physically significant peak of each radial distribution function thus obtaining the $k\chi_1(k)$ signal.

(iii) Distance information was easily obtained by first dividing the back-transformed signal by its amplitude envelope, followed by least-squares fitting of the sinusoidal term

$$\varphi(k,R) = \sin[2kR_1 + \psi_1(k)] \quad (5)$$

according to Ref. (*21*). To describe the phase shift function $\psi_1(k)$ we utilized the parametrized form proposed by Lee *et al.* (*22*). The experimental values of the parameters were extracted from reference compounds (Cu and CuO) constraining the R values to the crystallographic one without varying E_0, and then transferring these parameters to the catalyst samples, allowing variation of R and E_0. The latter adjustment is required for the definition of

$$k' = (k^2 + 0.262467\ \Delta E_0)^{1/2} \quad (6)$$

with k being defined by Eq. (3), and ΔE_0 corresponding to an energy shift with respect to a previously defined value, taking into account eventually an incomplete chemical phase transferability (*22*). The fittings were carried out in the 5–10 $Å^{-1}$ interval (k space).

(iv) The relative coordination numbers of catalysts and reference materials were obtained according to Sayers *et al.* (*23*) from the amplitude envelope of the FT^{-1} signal:

$$\ln\frac{A_r}{A_s} = \ln\frac{N_r}{N_s} + 2\ln\frac{R_s}{R_r} + 2(\sigma_s^2 - \sigma_r^2)k^2, \quad (7)$$

where r and s refer to reference compounds and samples, respectively. By fitting the resulting curve with a straight line function the intercept gives the ratio

$$\ln\left(\frac{N_r}{N_s}\cdot\frac{R_s^2}{R_r^2}\right),$$

while the slope defines the difference of the σ^2 values. All fits were conducted in the interval 25–100 $Å^{-2}$ in k^2 space.

In the case of one of the activated catalyst samples, a two-shell fit was carried out (vide infra) on the $k\chi_1(k)$ signal. The amplitude functions $F(k)$ for the model compounds (Cu and CuO) were parameterized in the Lorentzian form, as proposed by Teo *et al.* (*24*) for light backscatterer elements. The experimental parameters were calculated for the references fixing all known structural parameters and the previously

obtained phases at their respective values, and were then transferred to the sample signal. These fits were conducted in the range 5–11 $Å^{-1}$ in k space.

RESULTS

Copper Coordination

Moduli of the Fourier transform (FT) of the Cu K-edge EXAFS of fresh and activated (reduced) catalysts and of some references are given in Figs. 1 and 2. CuO shows

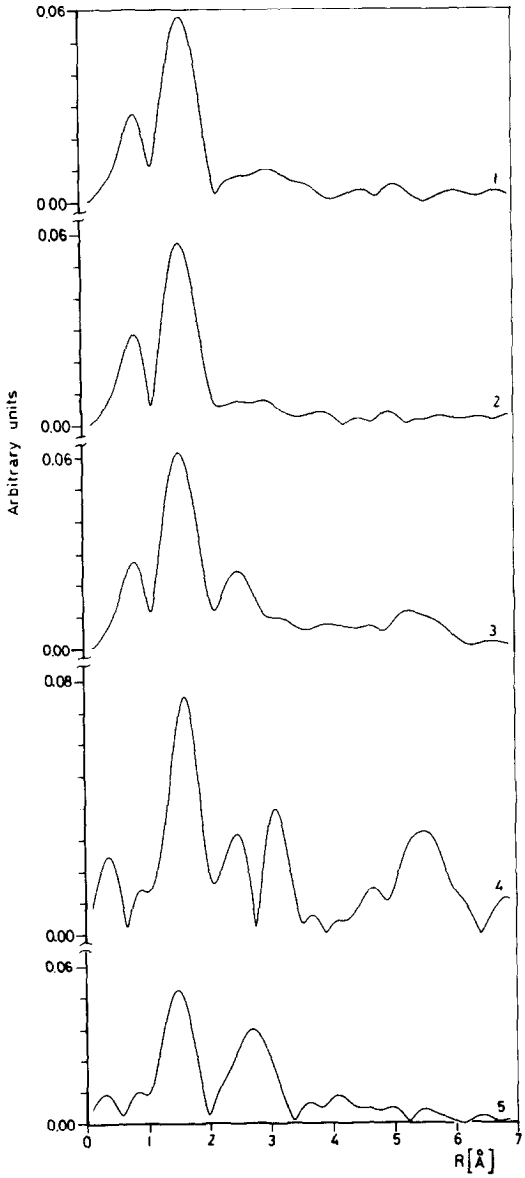

FIG. 1. Modulus of Fourier transform of Cu K-edge EXAFS spectra between k_{min} = 4.0 $Å^{-1}$ and k_{max} = 13.0 $Å^{-1}$. Curves 1–5: fresh Cu–ZnO/Al_2O_3, Cat. 1F, Cat. 2F and Cat. 3F, CuO, and Cu_2O, respectively.

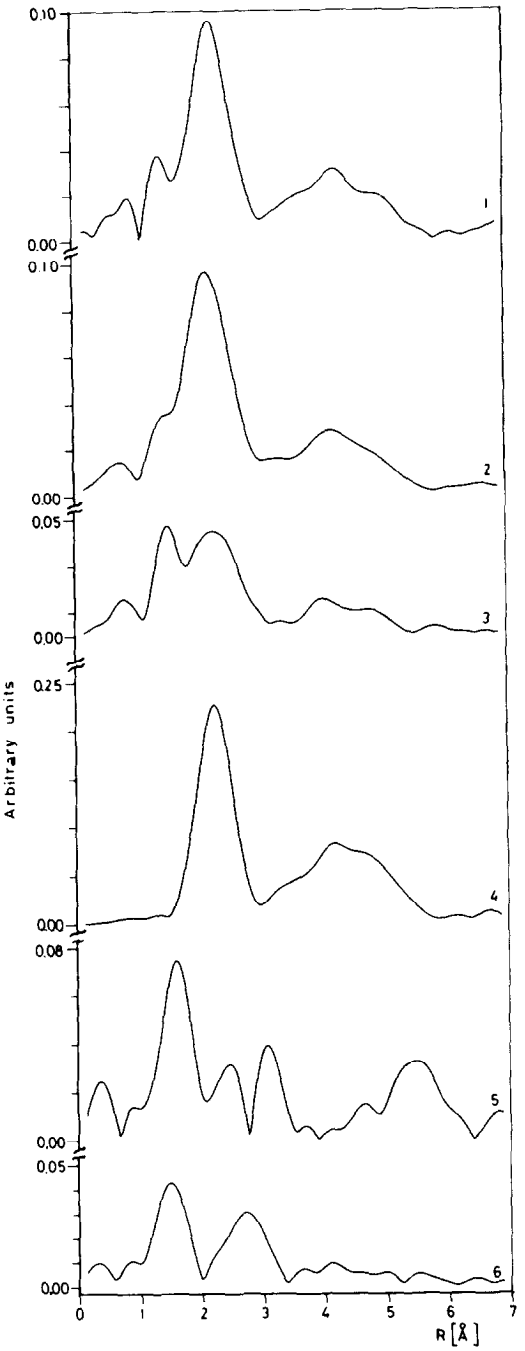

FIG. 2. Modulus of Fourier transform of Cu K-edge EXAFS spectra between k_{min} = 3.25 $Å^{-1}$ and k_{max} = 13.0 $Å^{-1}$ (curves 1–4) and k_{min} = 4.0 $Å^{-1}$ and k_{max} = 13.0 $Å^{-1}$ (curves 5–6). Curves 1–6: Activated Cu–ZnO/Al_2O_3, Cat. 1R, Cat. 2R and Cat. 3R, Cu, CuO, and Cu_2O, respectively.

three maxima, the first at 1.58 Å as compared to 1.50 Å in Cu_2O (crystallographic distances: 1.84 Å in Cu_2O, 1.95 Å in CuO). Fresh catalysts exhibit either one or two nearest-neighbor peaks with the first in the range 1.54–1.58 Å, but with considerable lower amplitude than for CuO, presumably as a result of high dispersion of the catalyst particles or a disordered structure.

Metallic copper (Fig. 2) shows a first shell well-separated from others at greater interatomic distances. Cat. 1R and Cat. 2R are essentially similar with maxima at 1.56 and 2.24 Å, whereas Cat. 3R shows two partially overlapping peaks at the same distances. The weak maximum at 1.56 Å (typical of Cu–O distances) in activated (reduced) catalysts is of interest and indicates oxidized states. In Cat. 1R and Cat. 2R the Cu–Cu amplitude of the 2.24-Å shell is three times lower than in the case of the metal; the effect is even more pronounced for Cat. 3R and may again be interpreted in terms of highly dispersed particles.

The first shells of the spectra of Fig. 1 were back-Fourier transformed according to Eqs. 4 and 5 and the function $\varphi_1(k,R)$ was determined. The experimental phase parameters for the Cu–O absorber–backscatterer pair were obtained by fitting this function for CuO with the crystallographically imposed Cu–O distance of 1.95 Å (*25*) (Table 2) and were then transferred to Cu_2O and the fresh catalyst samples. The resulting numerical results for R and ΔE_0 are given in Table 3 and the fits in Fig. 3. The calculated Cu–O distance in Cu_2O conforms to the crystallographic value (1.84 Å) (*26*); for the fresh catalyst samples we confirm the Cu–O distance typical of CuO.

Figure 4 reports the ratio of coordination numbers (according to Eq. (7)) of the three fresh catalyst samples with respect to CuO; a comparison with Cu_2O is included to test

TABLE 2

Fitted Experimental Absorber (Cu) and Backscatterer (O, Cu) Phase Parameters[a]

Parameter	Cu–O	Cu–Cu
$a_0 + b_0 - \pi$	2.59564	8.24409
$a_1 + b_1$ (Å)	−1.43222	−1.24460
$a_2 + b_2$ (Å^2)	0.04660	0.02595
$a_3 + b_3$ (Å^{-3})	−27.99720	−156.55279

[a] Phase shift function $\psi(k)$ in the parametrized form $\psi(k) = a_0 + b_0 - \pi + (a_1 + b_1)k + (a_2 + b_2)k^2 + (a_3 + b_3)/k^3$.

TABLE 3

Results of Fitting $\sin[2kR_1 + \psi_1(k)]$

Curve[a]	Sample	R_{Cu-O} (Å)	ΔE_0 (eV)
1	Cat. 1F	1.93(1)	0.9
2	Cat. 2F	1.94(1)	1.4
3	Cat. 3F	1.94(1)	3.3
4	CuO	1.95(—)	0
5	Cu_2O	1.84(1)	−1.4

[a] See Fig. 3.

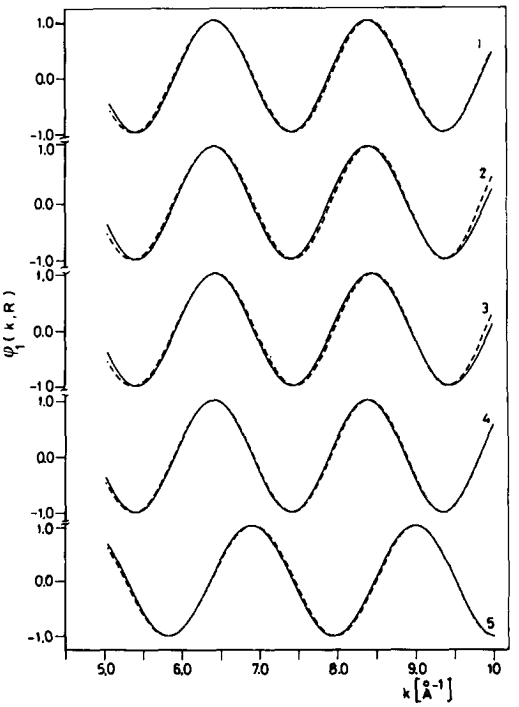

FIG. 3. Fit of $\varphi_1(k,R)$ vs k function for Cu–O distances in the range 5.0–10.0 Å^{-1} for Cu–ZnO/Al_2O_3, Cat. 1F, Cat. 2F and Cat. 3F, CuO, and Cu_2O (curves 1–5, respectively).

TABLE 4

Calculated Oxygen Coordination Numbers for Cu[a]

Curve[b]	Sample	$\ln\left[\frac{N_r}{N_s}\right] + 2\ln\left[\frac{R_s}{R_r}\right]$	N_s	$(\sigma_r^2 - \sigma_s^2)$ $(Å)^2$
1	Cat. 1F	0.330	2.87	−0.0011
2	Cat. 2F	0.372	2.75	−0.0012
3	Cat. 3F	0.121	3.54	0.0001
4	Cu_2O	0.618	1.92	−0.0008

[a] Referred to $N_r = 4$ for Cu in CuO.
[b] See Fig. 4.

the reliability of the experimental amplitudes. As shown in Table 4, N_{Cu} for Cu_2O is close to the theoretical value and within the commonly accepted experimental error (20%) (*27*). Also examination of the coordination numbers of the fresh catalyst samples conforms to the presence of a highly dispersed CuO phase. The same procedure has been applied to activated catalysts (Fig. 2). In view of the strong overlap in the Fourier transform of Cat. 3R antitransformation was carried out here in three different ranges to isolate the Cu–O contribution (first peak), the Cu–Cu contribution (second peak), and the Cu–O and Cu–Cu ensemble. Distance information was gained as above. Table 2 contains the experimental phase parameters obtained for the Cu–Cu atom pair in the metal by fitting $\varphi_1(k,R)$ using a fixed Cu–Cu distance (2.55 Å) (*28*). The resulting fits for the activated catalysts are given in Fig. 5 and R and ΔE_0 values in Table 5. For Cat. 3R the fit refers to the second peak at 2.24 Å. The numerical results for this sample are apparently not quite in line with the others; this is due to the errors induced by the cutoff at the minimum in FT at 1.82 Å. By back-transforming the 1.56-Å peak (due to the Cu–O atom pair) the fit of the corresponding $\varphi_1(k,R)$ function leads to R = 1.90(1) Å and ΔE = +3.4 eV. In order to improve the results for Cat. 3R we have also carried out a double-shell fitting on the $\chi(k) \cdot k$ vs k signal, taking

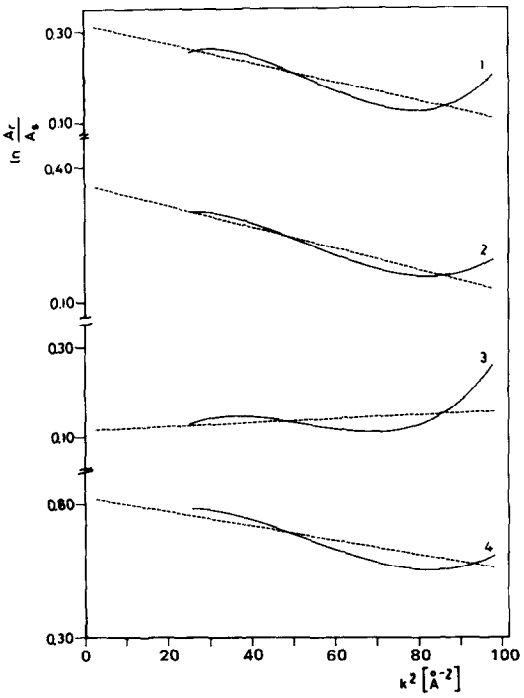

FIG. 4. Linear fit of curve of Eq. (7) vs k^2 (25–100 Å^{-2}) in fresh Cu–ZnO/Al_2O_3, Cat. 1F, Cat. 2F and Cat. 3F, and Cu_2O (curves 1–4, respectively) with respect to CuO.

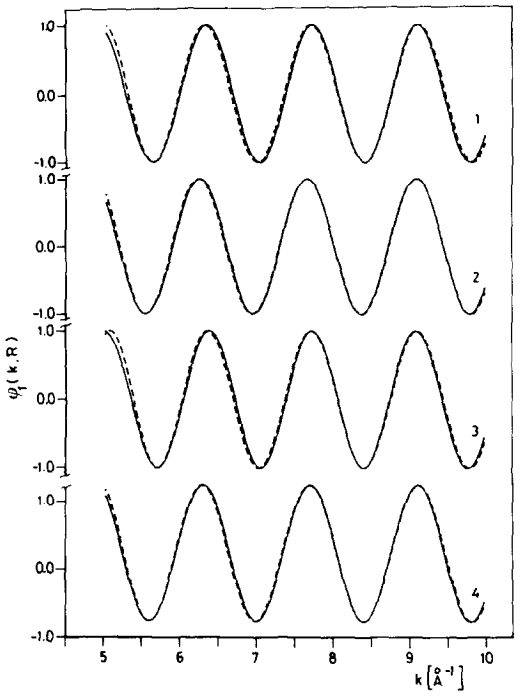

FIG. 5. Fit of $\varphi_1(k,R)$ vs k function for Cu–Cu distances in the range 5.0–10.0 Å^{-1} for Cu–ZnO/Al_2O_3, Cat. 1R, Cat. 2R and Cat. 3R, and Cu (curves 1–4, respectively).

TABLE 5

Results of Fitting $\sin[2kR_1 + \psi_1(k)]$

Curve[a]	Sample	R_{Cu-Cu} (Å)	ΔE_0 (eV)
1	Cat. 1R	2.56(1)	−3.0
2	Cat. 2R	2.55(1)	2.4
3	Cat. 3R	2.60(1)	−8.1
4	Cu	2.55(—)	0.0

[a] See Fig. 5.

the amplitude parameter values (*24*) from Cu and CuO. The parameters of CuO (Table 6) were transferred to Cu_2O for control (Table 5) and compared to literature values (*24*). As may be seen, **B** and **C** values are in good agreement, but the experimental value for **A** is about half the theoretical value (for an explanation, see note 13 of Ref. (*24*)). Figure 6 shows the double-shell fits for Cat. 3R, and the single-shell fitting for the nearest neighbors of metallic Cu and CuO. The beating at $k \approx 8.4$ Å^{-1} is due to the negative interference between the EXAFS signal of the two shells Cu–Cu and Cu–O. The values for Cat. 3R so obtained (Table 7) are now in good accordance with those of the other catalyst samples. Coordination numbers (referred to the metal) for Cu in all the activated samples are given in Table 8 and the fits according to Eq. (7) in Fig. 7 (for Cat. 3R the maximum at 2.24 Å was used). The low coordination numbers indicate again the presence of highly dispersed Cu(0).

TABLE 6

Parametrization of Amplitude Function $F(k)$[a,b]

Backscatterer	A (Å)		B (Å)		C (Å^{-1})	
	Expt	Theor	Expt	Theor	Expt	Theor
Cu	0.393	0.641	0.1980	0.1842	7.437	7.382
O	0.632	1.079	0.4100	0.4096	1.640	1.898

[a] Absorber: Cu.

[b] Amplitude function in the parametrized form $F(k) = A[1 + B^2(k - C)^2]^{-1}$.

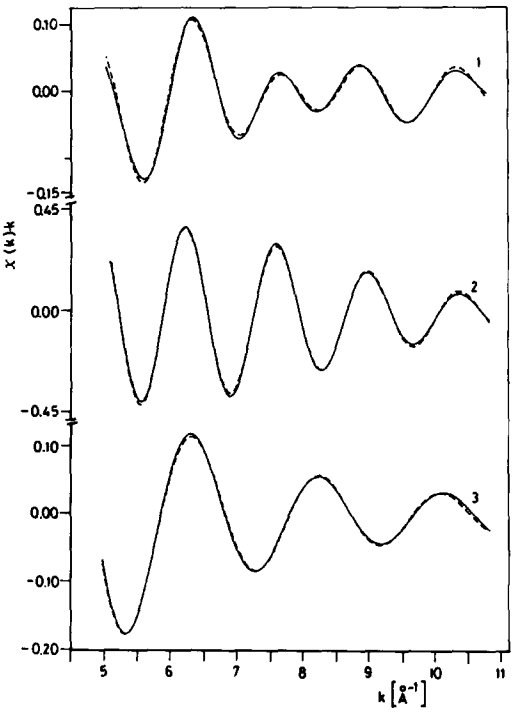

FIG. 6. Fit of the $\chi(k) \cdot k$ vs k signal in the range 5.0–11.0 Å^{-1} for Cu–ZnO/Al_2O_3, Cat. 3R, and Cu and CuO (curves 1–3, respectively).

Zinc Coordination

Figures 8 and 9 show the moduli of the FT of the Zn *K*-edge EXAFS spectra of fresh and activated catalysts in comparison with the references ZnO and $ZnAl_2O_4$. ZnO shows maxima at 1.60 and 2.76 Å, attributable to Zn–O and Zn–Zn peaks at 1.98 and 3.23 Å (*29, 30*) respectively. $ZnAl_2O_4$ is more structured with peaks at 1.52 Å (corresponding to Zn–O distances of 1.88 Å) and 3.20 Å (Zn–Al of 3.36 Å, Zn–O of 3.38 Å, and Zn–Zn of 3.51 Å (*31*)). The FT moduli of all fresh and activated catalysts contain two peaks, at 1.59 ± 0.03 and 2.80 ± 0.04 Å and confirm our earlier conclusion (*14*) that Zn is present only in the form of ZnO. No $ZnAl_2O_4$ spinel is found within the detection limits of EXAFS. It is noticed that the maximum of the first shell is considerably lower in the catalysts than in crystalline ZnO; for Cat. 1R and Cat. 2R there is also an inversion of peak heights for

TABLE 7

Results of Fitting the $\chi(k) \cdot k$ vs k Signal

Curve[a]	Sample	N_{Cu-O}	R_{Cu-O} (Å)	ΔE_0 (eV)	N_{Cu-Cu}	R_{Cu-Cu} (Å)	ΔE_0 (eV)
1	Cat. 3R	1.48	1.93(1)	−0.55	2.02	2.56(1)	−3.9
2	Cu	—	—	—	12.0	2.55(1)	0.0
3	CuO	4.0	1.95	0.0	—	—	—

[a] See Fig. 6.

the first and second shell. This denotes small dimensions of the ZnO particles and high structural disorder in the ZnO phase for the first two catalysts.

DISCUSSION

The literature suggests various copper states in Cu–ZnO/Al_2O_3 catalysts, namely as a metal (on the surface of Al_2O_3 or $ZnAl_2O_4$) (*32, 33*), or as Cu-containing compounds, such as spinels (*34–37*) or solid solutions of copper ions in ZnO or Al_2O_3 (*3, 4*). Reported phases are metastable solid solutions of Zn^{2+} and Al^{3+} ions in CuO, Cu^+ and Al^{3+} ions in ZnO, and (Cu, Zn)Al_2O_4 spinels. It appears that the spinel and CuO-based solid solutions do not determine the catalyst activity and that the high activity of Cu–ZnO/Al_2O_3 catalysts for methanol synthesis is associated with ZnO-based solid solutions (with introduction of Cu^+ and Al^{3+} (*3, 4, 38, 39*). On the other hand, Cu^+ species in solid solution with ZnO appear not to be greatly active in the CO shift reaction and Cu_2O (from oxidation of Cu(0)) is considered to be the active phase in LTS *reaction conditions* (*6*).

TABLE 8

Calculated Copper Coordination Numbers for Cu[a]

Curve[b]	Sample	$\ln\left[\frac{N_r}{N_s}\right] + 2\ln\left[\frac{R_s}{R_r}\right]$	N_s	$(\sigma_s^2 - \sigma_r^2)$ (Å)^2
1	Cat. 1R	0.807	5.35	0.0022
2	Cat. 2R	0.872	5.02	0.0015
3	Cat. 3R	1.713	2.16	−0.0001

[a] Referred to N_r = 12 in metallic copper.
[b] See Fig. 7.

In agreement with XANES data (*14*), EXAFS results of the fresh catalysts show two highly dispersed oxide phases, "ZnO" (i.e., ZnO or a ZnO–CuO solute) and "CuO" (i.e., CuO or a CuO–ZnO solute), in line with XRD data, which indicate "ZnO" and "CuO" with small particle size (Table 2). This is not surprising for Cat. 1, which was obtained from a single-phase hydrozincite precursor (*6*). Formation of such solutes is structurally possible on the basis of ionic radii criteria (r^{IV} Zn(II) = 0.60 Å; r^{IV} Cu(II) = 0.57 Å but r^{VI} Cu(II) = 0.73 Å

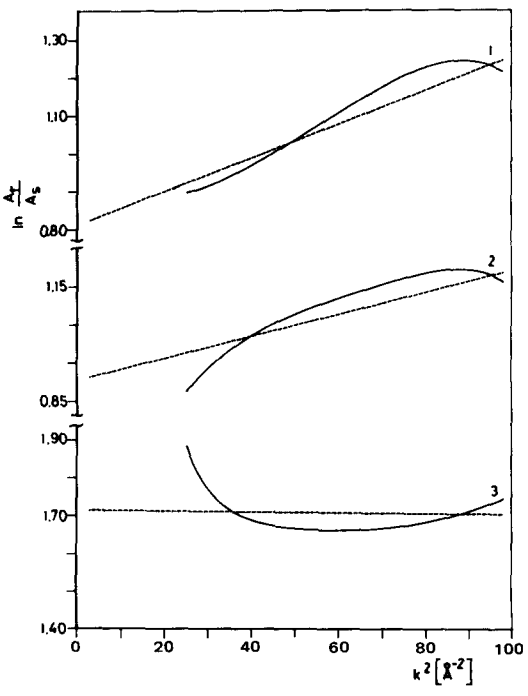

FIG. 7. Linear fit of curve of Eq. (7) vs k^2 (25–100 Å^{-2})in Cu–ZnO/Al_2O_3, Cat. 1R, Cat. 2R and Cat. 3R (curves 1–3, respectively) with respect to Cu.

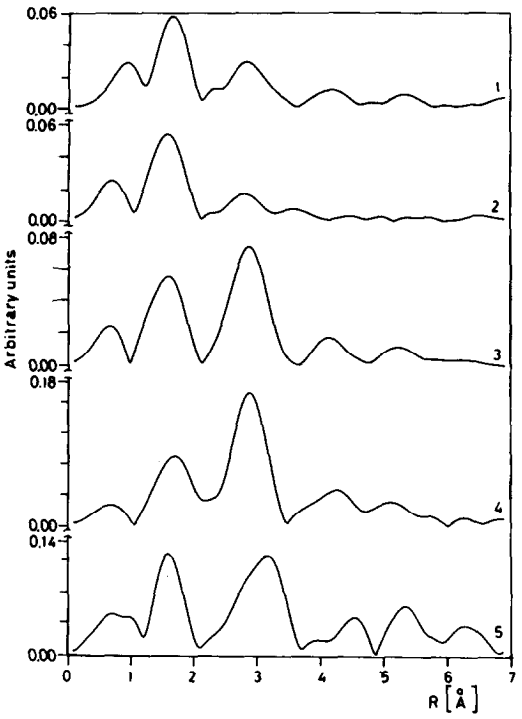

FIG. 8. Modulus of Fourier transform of Zn *K*-edge EXAFS spectra between $k_{min} = 3.9$ Å^{-1} and $k_{max} = 13.0$ Å^{-1}. Curves 1–5: fresh Cu–ZnO/Al_2O_3, Cat. 1F, Cat. 2F and Cat. 3F, ZnO, and $ZnAl_2O_4$, respectively.

(40)) and metal–oxygen distances. Whereas in ZnO the metal coordination polyhedron is an almost regular tetrahedron (3 × 1.973 and 1.992 Å) (*30*), CuO assumes a highly distorted octahedral (4 + 2) coordination for the metal, which is essentially square planar (2 × 1.951 and 2 × 1.961 Å) with two remote oxygens (2.784 Å) (*25*). The solubility of CuO in wurtzite is therefore limited to about *5%* (*7, 41, 42*), and the resulting quite small decrease in the *c* dimension escapes detection in the line-broadened XRD pattern. Indications for a solid solution of ZnO in CuO ("CuO") are also available (*43*). It is also known that Cu_2O layers form with ZnO inclusions for [Zn] < 15% by passivation of CuZn alloys (*44*). Detection of the solutes in low amounts by means of Cu *K*- and Zn *K*-edge EXAFS in the presence of excess CuO and ZnO appears arduous. Dissolution of small amounts (2–4%) of CuO in ZnO in Cat. 1 is confirmed by XPS results (*6*).

Whereas diffraction work fails to ascertain compound formation (spinels) in our samples, EXAFS shows evidence for the absence of $ZnAl_2O_4$, at least in detectable quantities. Formation of a considerable fraction of MAl_2O_4 spinels (M = Cu, Zn) was previously already excluded for the same samples on the basis of the near-edge structure (*14*).

Activated samples have been subjected to temperature treatment in a reductive medium. Although low-temperature reduction does not affect ZnO in Cu–ZnO/Al_2O_3 catalysts the compound delays hydrogen reduction of CuO, a process which usually takes place in two stages (to Cu via Cu_2O) at low temperature (<200°C); at higher temperature no Cu_2O is formed (*45*), in accordance with our XRD, XANES, and EXAFS indications. By reduction at about 300°C brass

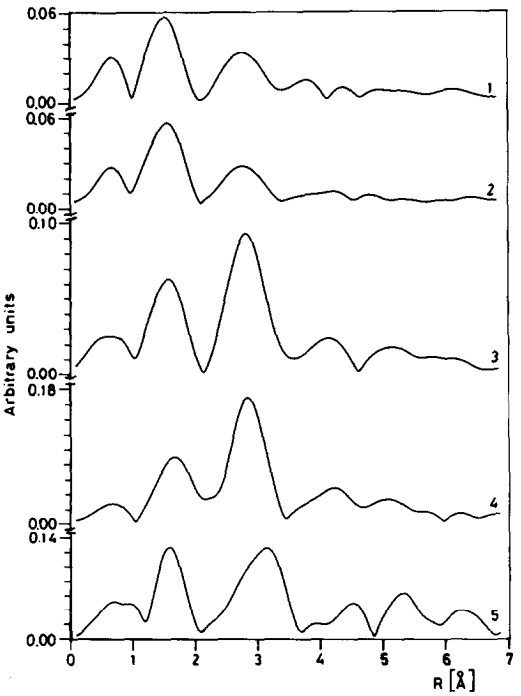

FIG. 9. Modulus of Fourier transform of Zn *K*-edge EXAFS spectra between $k_{min} = 3.9$ Å^{-1} and $k_{max} = 13.0$ Å^{-1}. Curves 1–5: activated Cu–ZnO/Al_2O_3, Cat. 1R, Cat. 2R and Cat. 3R, ZnO, and $ZnAl_2O_4$, respectively.

may be formed (*8*), but is excluded in our case.

The presence of Cu as the backscattering element in the first and probably in the second coordination shell is confirmed by the EXAFS signal of the reduced catalysts (Fig. 2). The decreased signal intensity with respect to metallic copper indicates a variation of the scattering amplitude, probably as a result of a decrease in coordination number due to the reduced dimensions of the metallic clusters. This is in accordance with the fact that fine dispersions of metallic copper have been reported in other 10–30% copper catalysts (*46*) (as in our case) and relatively large copper crystals in richer systems (*4*). It thus appears that we are dealing with a fine copper dispersion in contact with ZnO (copper-containing or not). At this point we notice that Cu(0) is easily trapped in a ZnO layer, as shown by Okamoto *et al.* (*47*) for reduced Cu–ZnO catalysts and by Barr and Hackenberg (*44*) for passivation of CuZn alloys.

It has been claimed that activated Cu–ZnO/Al_2O_3 catalysts contain two forms of copper, one appearing in and strongly interacting with the zinc oxide phase (further designated as "ZnO–R") and the other being a fine copper metal dispersion acting as a weak electron donor to zinc oxide (*4, 48*). The structure of "ZnO–R" has been indicated as a solute of Cu(I) in ZnO. This conjecture is based on the following considerations:

(a) Cu(I) fits in with a mechanism of the catalytic function (in methanol formation) via chemisorption and activation of CO on Cu(I) centers and of hydrogen on the surrounding ZnO surface (*4*).

(b) Cu(I) explains the stabilizing action of Al_2O_3 by maintaining electroneutrality according to

$$\text{Zn(II)} \rightleftharpoons \text{Cu(I)} + \text{Al(III)}$$

It appears that ZnO stabilizes catalytically active Cu(I) (*49*).

(c) NIR–VIS absorption spectrum of Cu(I)/ZnO differs from Cu(II)/ZnO (*3, 50*).

(d) Cu(I) is isoelectronic with Zn(II).

(e) Cu(I) frequently assumes a tetrahedral coordination (*47*) (though rarely with an oxygen environment).

(f) Support from the Cu(I)–O bond-strength (*s*) bond-length (*d*) relation. Namely, if we consider the *s–d* relation for Cu(I)–S (*51*) and bond data for $Cu_2^{I}SO_3 \cdot Cu^{II}SO_3 \cdot 2H_2O$(Cu(I)–S, 2.14 Å, Cu(I)–O, 2.11–2.14 Å), Cu_2O, $CuCrO_2$, and $SrCu_2O_2$ (Cu–O, 1.84–1.85 Å) (*26, 52, 53*), the derived equation $s = (d/1.686)^{-7.9}$ can be used to predict a tetrahedral Cu(I)–O bond length of 2.01 Å, close to the mean Zn–O length of 1.98 Å in ZnO.

On the whole, the proposed Cu(I)–ZnO phase with crystallographic parameters almost indistinguishable from ZnO (*4*) is a highly acceptable hypothesis. Consequently, and also as reduction drives more copper into zinc oxide (up to 16% in a Cu/ZnO = 30/70 catalyst, close to the composition ratio in our samples) (*3, 4, 54*), this aspect was carefully considered in the interpretation of the X-ray absorption spectra. Chemical shifts in the *K* absorption edge value for Cu (ΔE_K (Cu)) in reduced Cu–ZnO/Al_2O_3 catalysts (Table 2, Ref. (*14*)) are compatible with both Cu(0) and Cu(I) valence states (*14*), but in the latter case only with Cu_2O for which the unique cubic structure with linear oxygen coordination leads to an atypical ΔE_K Cu(I) value (*55*). While the antiphase features of the XANES spectra of Cu_2O and reduced catalysts at the high-energy side of the Cu *K* absorption edge exclude the presence of Cu(I) as Cu_2O, the EXAFS signals of the reduced catalysts show mainly Cu instead of O as the scattering element in the first and probably in the second shell. This reduces greatly the incidence of the Cu(I)–ZnO hypothesis for our samples. If one considers, however, that monovalent Cu species are expected especially for low Cu content coprecipitated catalysts they should therefore not be abundant in our case and may be below the detection limits. In the case of Cat. 3R the strong evidence

for residual CuO may be the result of incomplete reduction, eventually by inaccessibility of CuO to the reducing gas by a ZnO shield.

CONCLUSIONS

Fresh Cu–ZnO/Al_2O_3 catalysts contain CuO and ZnO in a state of considerable structural disorder. The presence of CuO–ZnO solutes (XPS evidence) cannot be dismissed from EXAFS data but neither confirmed. Reduced (*ex situ*) catalysts contain a fine copper dispersion in contact with ZnO, but no Cu_2O. In one case the reduced catalyst was found to contain considerable amounts of residual CuO. The interpretation of the results should take into account the detection limits of the method which is not expected to be sensitive to low-concentration phases in the presence of other main phases and may explain the fact that no spinels and Cu(I)–ZnO solutes were observed.

ACKNOWLEDGMENTS

The authors gratefully acknowledge technical assistance of the staff of the Frascati ADONE and PULS Laboratories. Dr. G. Petrini (Ausind, Montedison Group, Novara) kindly supplied the catalyst samples.

REFERENCES

1. Thomas, C. L., "Catalytic Processes and Proven Catalysts," Academic Press, New York, 1970.
2. Shimomura, K., Ogawa, K., Oba, M., and Kotera, Y., *J. Catal.* **52,** 191 (1978).
3. Herman, R. G., Klier, K., Simmons, G. W., Finn, B. P., Bulko, J. B., and Kobylinski, T. P., *J. Catal.* **56,** 407 (1979).
4. Mehta, S., Simmons, G. W., Klier, K., and Herman, R. G., *J. Catal.* **57,** 339 (1979).
5. Shishkov, D. S., Kasabova, N. A., Andreev, A. A., and Shopov, D. M., *in* "Heterogeneous Catalysis; Proceedings, 4th International Symposium on Heterogeneous Catalysis, Part 1, Varna, 1979" (D. M. Shopov, A. A. Andreev, A. Palazov, and L. Petrov, Eds.), p. 169. Bulgarian Academy of Sciences, Sofia, 1979.
6. Petrini, G., Montino, F., Bossi, A., and Garbassi, F., *in* "Preparation of Catalysts III" (G. Poncelet, P. Grange, and P. A. Jacobs, Eds.), p. 735. Elsevier, Amsterdam, 1983.
7. Schiavello, M., Pepe, F., and De Rossi, S., *Z. Phys. Chem.* **92,** 109 (1974).
8. van Herwijnen, T., and de Jong, W. A., *J. Catal.* **34,** 209 (1974).
9. Campbell, J. S., *I & EC Process Des. Dev.* **9,** 588 (1970).
10. Young, P. W., and Clark, C. B., *Chem. Eng. Prog.* **69,** 69 (1973).
11. Uchida, H., Isogai, N., and Oba, M., *J. Chem. Soc. Jpn. Ind. Chem. Sect.* **72,** 2195 (1969).
12. Uchida, H., Oba, M., Isogai, N., and Hasegawa, I., *Bull. Chem. Soc. Jpn.* **41,** 479 (1968).
13. Völter, J., Berndt, H., and Lietz, G., *Chem. Technol.* **28,** 606 (1976).
14. Vlaic, G., Bart, J. C. J., Cavigiolo, W., and Mobilio, S., *Chem. Phys. Lett.* **76,** 453 (1980).
15. Balzarotti, A., Comin, F., Incoccia, L., and Mobilio, S., unpublished.
16. Bearden, J. A., and Burr, A. F., *Rev. Mod. Phys.* **39,** 125 (1967).
17. Stern, E. A., Sayers, D. E., and Lytle, F. W., *Phys. Rev. B* **11,** 4836 (1975).
18. Vlaic, G., Bart, J. C. J., Cavigiolo, W., Mobilio, S., and Navarra, G., *Chem. Phys.* **64,** 115 (1982).
19. Vlaic, G., and Bart, J. C. J., *Rec. Trav. Chim.* **101,** 171 (1982).
20. Lonsdale, K., Ed., "International Tables for X-Ray Crystallography," Vol. 3, p. 161. Kynoch Press, Birmingham, 1972.
21. Vlaic, G., Bart, J. C. J., Cavigiolo, W., Mobilio, S., and Navarra, G., *Z. Naturforsch. A* **36,** 1192 (1981).
22. Lee, P. A., Teo, B. K., and Simons, A. L., *J. Amer. Chem. Soc.* **99,** 3856 (1977).
23. Sayers, D. E., Stern, E. A., and Lytle, F. W., *Phys. Rev. Lett.* **35,** 584 (1975).
24. Teo, B. K., Lee, P. A., Simons, A. L., Eisenberger, P., and Kincaid, B. M., *J. Amer. Chem. Soc.* **99,** 3854 (1977).
25. Åsbrink, S., and Norrby, L. J., *Acta Crystallogr. Sect. B* **26,** 8 (1970).
26. Neuburger, M. C., *Z. Phys.* **67,** 845 (1931).
27. Hunter, S. H., Ph. D. thesis. Stanford University, SSRP Report N77/4 (1977).
28. Pearson, W. B., "A Handbook of Lattice Spacings and Structures of Metals and Alloys," p. 125. Pergamon, London, 1958.
29. Sabine, T. M., and Hogg, S., *Acta Crystallogr. Sect. B* **25,** 2254 (1969).
30. Abrahams, S. C., and Bernstein, J. L., *Acta Crystallogr. Sect. B* **25,** 1233 (1969).
31. Saalfeld, H., *Z. Kristallogr.* **120,** 476 (1964).
32. Ogino, Y., Oba, M., and Ochida, H., *Bull. Chem. Soc. Jpn.* **33,** 358 (1960).
33. Tsybina, E. N., *Khim. Prom. (Moscow)* **3,** 257 (1973).
34. Natta, G., *Catalysis* **3,** 349 (1955).
35. Prudnikova, O. Yu., Makarova, O. V., and Yurieva, T. M., *React. Kinet. Catal. Lett.* **14,** 413 (1980).

36. Shishkov, D. S., Kassabova, N. A., and Petkov, K. N., *in* "Preparation of Catalysts III" (G. Poncelet, P. Grange, and P. A. Jacobs, Eds.), p. 757. Elsevier, Amsterdam, 1983.
37. Wang Ching, Lu Jin, Chen Wu-zheng, Chang Zu-shuo, and Zhu Wei, *in* "Proceedings, China–Japan–USA Symposium on Heterogeneous Catalysis," p. A230. Dalian, 1982.
38. Kuznetsova, L. I., Yurieva, T. M., Minyukova, T. P., Ketchik, S. V., Plyasova, L. M., and Boreskov, G. K., *React. Kinet. Catal. Lett.* **19,** 355 (1982).
39. Ketchik, S. V., Minyukova, T. P., Kuznetsova, L. I., Plyasova, L M., Yurieva, T. M., and Boreskov, G. K., *React. Kinet. Catal. Lett.* **19,** 345 (1982).
40. Shannon, R. D., *Acta Crystallogr. Sect. A* **32,** 751 (1976).
41. Délorme, C., *Bull. Soc. Fr. Mineral. Cristallogr.* **81,** 26 (1958).
42. Chapple, F. H., and Stone, F. S., *Proc. Brit. Ceram. Soc.* **1,** 45 (1964).
43. Garbassi, F., and Petrini, G., Paper presented at Third National Meeting on Catalysis. Rimini, 1982.
44. Barr, T. L., and Hackenberg, J. J., *Appl. Surf. Sci.* **10,** 523 (1982).
45. Ruggeri, O., Trifirò, F., and Vaccari, A., *J. Solid State Chem.* **42,** 120 (1982).
46. Semenova, T. A., Lyudkovskaya, B. G., Markina, M. I., Volynkina, A. Ya., Cherkasov, G. P., Sharkina, V. I., Khitrova, N. F., and Shpiro, G. P., *Kinet. Catal.* **18,** 834 (1977).
47. Okamoto, Y., Fukino, K., Imanaka, T., and Teranishi, S., *J. Chem. Soc. Chem. Commun.*, 1406 (1982).
48. Herman, R. G., Simmons, G. W., and Klier, K., *in* "Proceedings, 7th International Congress on Catalysis, Tokyo, 1980," p. 475. Kodansha/Elsevier, Tokyo/Amsterdam, 1981.
49. Henrici-Olivé, G., and Olivé, S., *J. Mol. Catal.* **17,** 89 (1982).
50. Weakliem, H. A., *J. Chem. Phys.* **36,** 2117 (1962).
51. Brown, I. D., *in* "Structure and Bonding in Crystals" (M. O'Keeffe and A. Navrotsky, Eds.), Vol. II, p. 1. Academic Press, New York, 1981.
52. Dannhauser, W., and Vaughan, P. A., *J. Amer. Chem. Soc.* **77,** 896 (1955).
53. Teske, C. L., and Müller-Buschbaum, Hk., *Z. Anorg. Allg. Chem.* **379,** 113 (1970).
54. Bulko, J. B., Herman, R. G., Klier, K., and Simmons, G. W., *J. Phys. Chem.* **83,** 3118 (1979).
55. Murugesan, T., Sarode, P. R., Gopalakrishnan, J., and Rao, C. N. R., *J. Chem. Soc. Dalton*, 837 (1980).